Effects of Gas Velocity on Deposition Rate and Amount of Cluster Incorporation into a-Si:H Films Fabricated by SiH_4 Plasma Chemical Vapor Deposition*)

Takashi KOJIMA, Susumu TOKO, Kazuma TANAKA, Hyunwoong SEO, Naho ITAGAKI, Kazunori KOGA and Masaharu SHIRATANI

Department of Electronics, Kyushu University, Fukuoka 819-0395, Japan

(Received 7 January 2018 / Accepted 30 January 2018)

To deposit stable a-Si:H films at a high deposition rate (*DR*), we have studied time evolution of *DR* and amount of cluster incorporation (*R*) into films as a parameter of gas velocity, in the downstream region of a multi-hollow discharge plasma chemical vapor deposition reactor; because a-Si:H films containing less cluster incorporation show high stability. For a low gas velocity of 0.18 m/s, clusters are trapped between the multi-hollow electrode and the substrate and the trapped clusters absorb clusters and such absorption suppresses the cluster incorporation into films. By utilizing this phenomenon, we have realized a quite low $R = 1.3$ at a high $DR = 0.06$ nm/s.

Keywords: plasma CVD, cluster, a-Si:H, solar cell, laser light scattering, quartz crystal microbalance

DOI: 10.1585/pfr.13.1406082

1. Introduction

50 billion Internet of Things (IoT) devices installed by 2020 will change life as we know it [1, 2]. However, the problem of powering these huge number of devices is unsolved [1, 2]. Most of these smart devices use batteries as their source of energy. The replacement of the batteries often is one key limiting factor for the devices because of cost and environmental implication.

Hydrogenated amorphous silicon (a-Si:H) solar cell is a potential energy harvesting device for IoT [3–7]. Solar harvesting is well-suited for the devices that are installed outdoor and exposure to light. Flexible solar cells can also be used for indoor sensors and wearable devices. Many a-Si:H solar cells, indeed, are used in watches and calculators. However, one of the biggest challenges to use a-Si:H solar cell for IoT devices is the problem of its low stability. Si cluster incorporation into a-Si:H films during the films deposition is the main cause for light-induced degradation (LID) and LID leads to a significant reduction of the efficiency of the a-Si:H solar cell [7, 8]. A-Si:H film is deposited mostly using SiH_4 plasmas. In SiH_4 plasmas, SiH_3, SiH_2, SiH, Si, H_2 and H are generated by electron impact dissociation of SiH_4 molecules [7, 8]. SiH_3 radicals have a long lifetime, and they are main deposition precursors for high quality a-Si:H films [9–12]. Other radicals have a short lifetime, and they are minor deposition species. Among these short lifetime radicals, SiH_2 radicals contribute significantly to Si cluster generation [13, 14]. The LID tends to be reduced with decreasing a density of Si-H_2 bonds in films [15–19]. There are two origins of Si-H_2 bonds in films: one is surface reactions of SiH_3 radicals and the other is the incorporation of clusters. Normally, cluster incorporation is the main origin of Si-H_2 bonds in films [20–23]. Therefore, the suppression of cluster incorporation into films is the key to realizing highly stable a-Si:H films.

We have developed a multi-hollow discharge plasma CVD (MHDPCVD) method in which cluster incorporation is suppressed using gas flow. We have also developed a quartz crystal microbalance (QCM) method which offers information on the deposition rate (*DR*) and the amount of cluster incorporation into films (*R*), being the ratio of the total deposition rate to the radical deposition rate [24–28]. In the upstream region of the MHDPCVD reactor, we have realized high sensitivity measurement of cluster incorporation by the QCM method. Based on the results, we have deposited a-Si:H films of low *R* of 3 at a deposition rate of 0.09 nm/s [29]. Here, we studied the time evolution of amount of clusters, *DR* and *R* in the downstream region of the MHDPCVD reactor using a laser light scattering (LLS) method together with the QCM method. We found that clusters are trapped in the downstream region, and we realized a very low *R* of 1.3 with a *DR* of 0.06 nm/s.

2. Experimental

Experiments were carried out with a MHDPCVD reactor equipped with QCMs. Figure 1 (a) shows a schematic of the experimental setup. Plasmas were sustained in 79

author's e-mail: koga@ed.kyushu-u.ac.jp

*) This article is based on the invited talk at the 33rd JSPF Annual Meeting (2016, Tohoku).

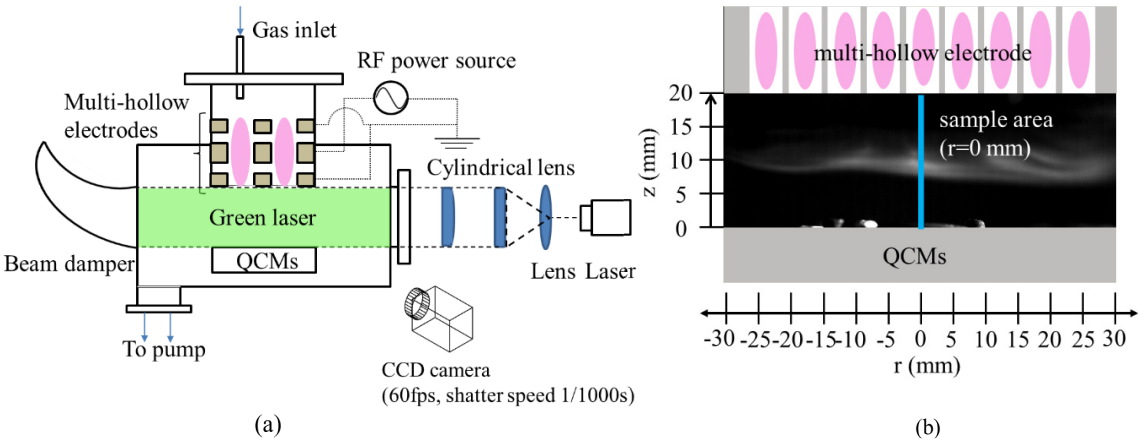

Fig. 1 (a) Multi-hollow discharge plasma reactor with QCMs and LLS setup. (b) Typical snap shot of LLS intensity and configuration of electrode and QCMs.

holes of the electrodes. The diameter and length of the holes are 5.0 mm and 9.8 mm. The powered electrode was connected to a 60 MHz rf power source through a matching network, which reduces the reflected power to 0 W in all experiments. Pure SiH_4 was fed through the upper side of the reactor, then passed through the holes in the electrodes, and pumped out. The gas flow rate of SiH_4 was set in a range of 10 to 70 sccm (gas velocity = 0.18 to 1.28 m/s). The total pressure was 0.5 Torr. The gas temperature was 20°C (= 293 K). The discharge power was 20 W. Si clusters generated in plasmas were transported towards the downstream region by the gas flow, because their diffusion velocity was less than the gas velocity. Therefore, we can realize a cluster-rich condition in the downstream region.

To measure *DR* and *R*, we employed three QCMs which were set at 20 mm below the lowest electrode. The temperature of these QCMs was kept at 373 ± 0.05 K with a high-precision temperature controller (Thermo Scientific, NESLAB RTE740). A sheet beam of second harmonics of YAG laser light (λ = 532 nm, 320 mW) was passed through the space between the electrode and QCMs. The width of the sheet beam was 20 mm. 90° Rayleigh scattering intensity from clusters was measured with a high speed camera (Photron, FASTCAM SA-X PI4) with a frame rate and shutter speed were 60 fps and 1/1000 s, respectively. Figure 1 (b) shows a typical snap shot of LLS intensity and the sample area. The spatiotemporal evolution of Si cluster transportation was measured in this sample area of r = 0 mm and z = 0 - 20 mm, where r = 0 mm was the center of multi-hollow electrodes and z = 0 mm was the surface of QCMs.

3. Results and Discussion

Two different types of cluster transport were observed in this study. Figures 2 (a) and (b) show the cluster transports at 2, 50, 120 s after the plasma ignition, for the gas velocity of 0.18 and 0.73 m/s. For 0.18 m/s, and t = 2 s, clusters are trapped between the multi-hollow electrode and the substrate. Then, the clusters are driven towards the QCMs by gas flow and the LLS intensity decreases from t = 50 s. However, for 0.73 m/s, the clusters are not trapped and they begin to be transported towards the QCMs just after the plasma ignition.

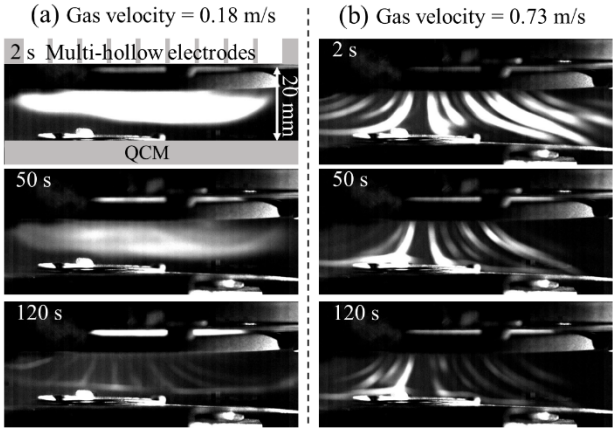

Fig. 2 Snap shots of LLS intensity for gas velocity of 0.18 and 0.73 m/s.

We measured the time evolution of total deposition rate (DR_{total}), radical deposition rate ($DR_{radical}$) and *R* as a parameter of the gas velocity in the downstream region. DR_{total} increases with time as shown in Fig. 3 (a). For the gas velocity of 0.73 m/s or more, the DR_{total} is saturated at around 0.1 nm/s. However, for the gas velocity of 0.18 m/s, the DR_{total} decreases slightly during t = 40 - 60 s and then increases again. Figure 3 (b) shows the time evolution of $DR_{radical}$. For the gas velocity of 0.18 m/s, the $DR_{radical}$ increases to 0.06 nm/s after turning on the discharge, then decreases to 0.02 nm/s. This decrease in $DR_{radical}$ is the main reason for the decrease of DR_{total} during t = 40 - 60 s.

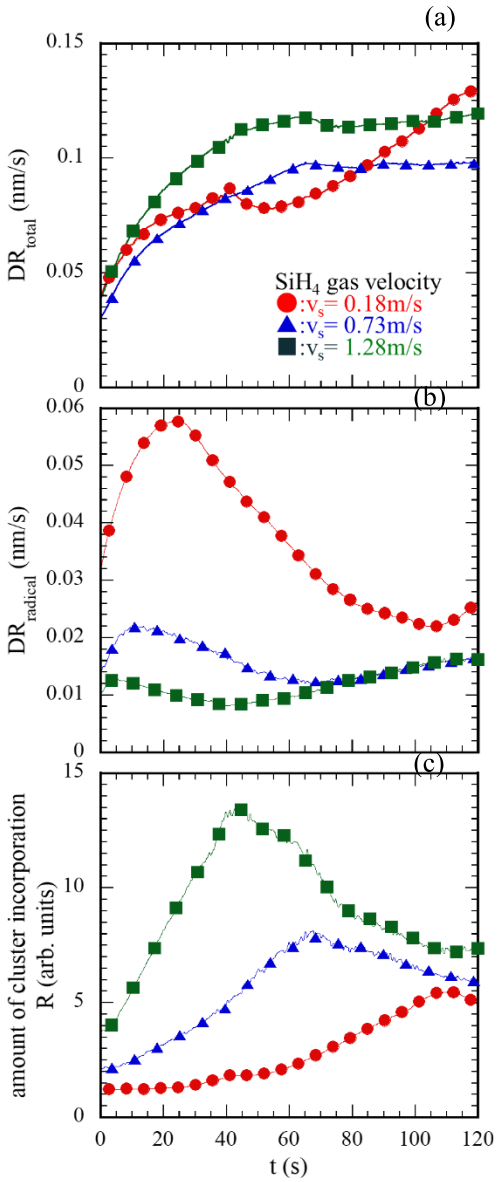

Fig. 3 Time evolution of (a) DR_{total}, (b) DR_{radical}, and (c) R.

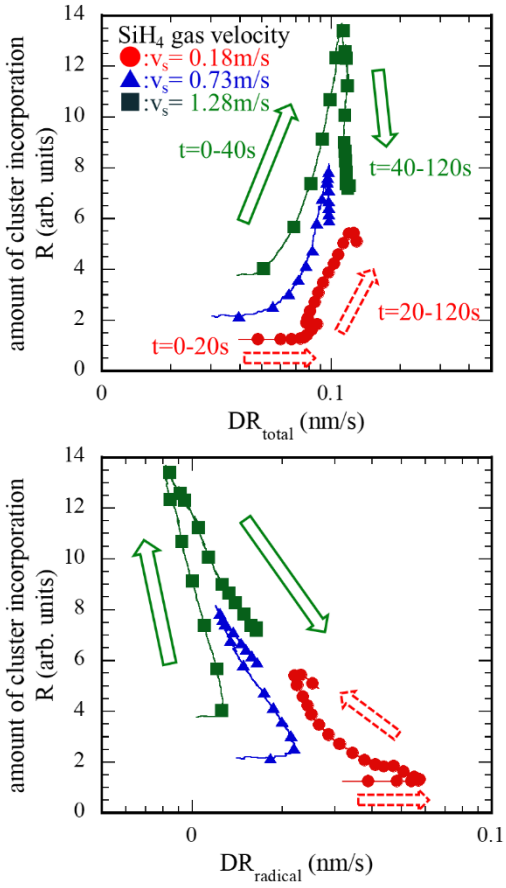

Fig. 4 Relationship between R and DR.

As the gas velocity increases, the increase in DR_{radical} becomes small and it is nearly constant for the gas velocity of 1.28 m/s. These results suggest that the transport of radicals and clusters are affected by gas velocity, and the slow gas velocity promotes DR_{radical} in the initial discharge phase. This influence is not due to neutral collisions because the diffusion velocity of the radical is faster than the gas velocity.

R increases with time as shown in Fig. 3 (c). For the gas velocity of 0.73 m/s or more, R increases immediately after the discharge ignition, whereas for the gas velocity of 0.18 m/s, R remains low during t = 0 - 50 s. This occurs when the clusters are trapped between the multi-hollow electrode and the substrate. These results suggest that trapped clusters suppress the cluster incorporation.

Figure 4 shows the relationship between DR and R. We realized a quite low R of 1.3 with a high DR_{radical} of 0.06 nm/s for the gas velocity of 0.18 m/s. DR and R show nonlinear dependence on time. These nonlinear dependence is caused by the fact that 1) the cluster transport changes with time, and affects directly R and DR_{total}. 2) clusters reduce DR_{radical} owing to radical loss to clusters. DR_{total}, R can be written as;

$$DR_{\text{total}} = DR_{\text{cluster}} + DR_{\text{radical}} \times \frac{1}{T_{\text{radical}}}, \tag{1}$$

$$R = \frac{DR_{\text{total}}}{DR_{\text{radical}}}, \tag{2}$$

where DR_{cluster} is deposition rate of cluster, T_{radical} is SiH_3 radical transmittance of cluster eliminating filter. When DR_{radical} is sufficiently small, DR_{total}, R has strong correlation with the amount of cluster transport to the substrate.

DR_{radical} is generally proportional to n_{SiH3} of SiH_3 radical density. Under a low gas flow rate and a high discharge power, DR_{radical} is reduced owing to radical loss to the clusters. Taking this loss process into account, the theoretical equation is obtained from the following rate equation of SiH_3 radicals;

$$\frac{dn_{\text{SiH}_3}}{dt} = k_{\text{SiH}_3} n_e n_s - D\nabla^2 n_{\text{SiH}_3} - k_{\text{cr}} n_c n_{\text{SiH}_3} - \frac{n_{\text{SiH}_3}}{\tau_{\text{SiH}_3}}, \tag{3}$$

where k_{SiH3} is the generation rate coefficient of SiH_3, n_e is

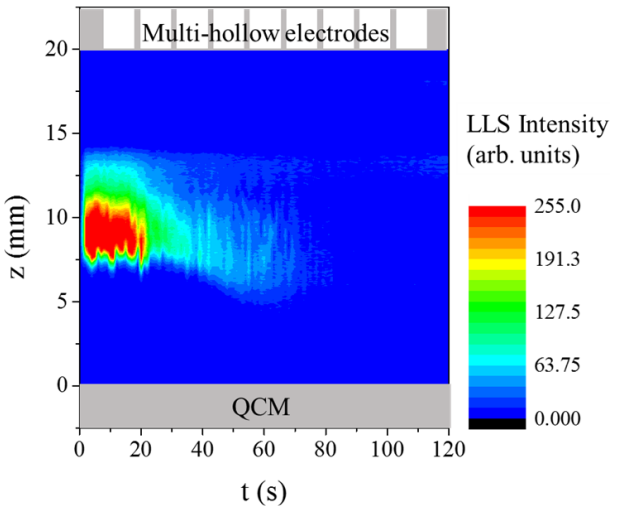

Fig. 5 Spatiotemporal distribution of LLS intensity.

the electron density, n_s is the SiH_4 gas density, D is the diffusion coefficient of radicals, k_{cr} is the coefficient of SiH_3 radical loss rate to cluster, n_c is the cluster density, τ_{SiH3} is the residence time of SiH_3 radical according with gas velocity. The influence of gas flow on radicals is small under the present experimental conditions. Electron density and gas density depend on the discharge power and pressure, respectively. Thus, the time evolution of $DR_{radical}$ depends mainly on the radical loss to clusters represented by the third term on the right hand of Eq. (3). For the gas velocity of 0.18 m/s, the existence area of clusters becomes narrower due to the cluster trapping, and the radical loss decreases during t = 0 - 20 s.

Figure 5 shows the spatiotemporal distribution of LLS intensity between the electrodes and the substrate, for the gas velocity of 0.18 m/s. Clusters exist above 7 mm from QCMs, just after turning on the discharges and they gradually are transported down toward the QCMs from t = 30 s. This result suggests that after the plasma ignition, some forces act on the cluster in the direction opposite to the gas flow, and the forces become weak from t = 30 s. In the downstream region of MHDPCVD reactor, the forces acting on cluster are gravity, thermophoretic force, gas drag force and, electrostatic force due to electric field for the charged clusters.

Gravity is given by,

$$F_g = \frac{\pi d_c^3 \rho_c g}{6}, \tag{4}$$

where g is acceleration of gravity, d_c is the cluster diameter, and ρ_c is its mass density.

The thermophoretic force can be written as;

$$F_T = -\frac{2\sqrt{2\pi} d_c^2}{15 v_{ts}} \left[1 + \frac{5\pi}{32}(1-\alpha)\right] \kappa_t \nabla T_s, \tag{5}$$

where κ_t is the translational part of the thermal conductivity, α is the accommodation coefficient, ∇T_s is the temperature gradient in the SiH_4 gas, and v_{ts} is the average thermal speed of SiH_4 gas molecules given by,

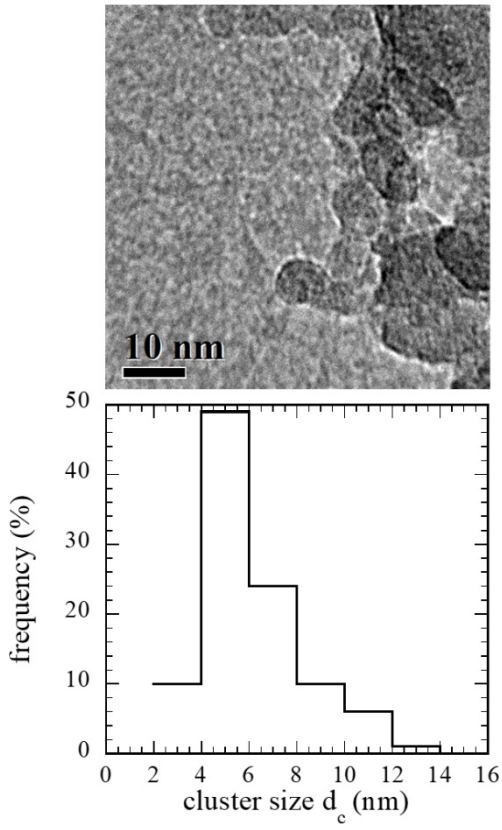

Fig. 6 TEM images of clusters in the downstream region and histograms of the cluster size distribution.

$$v_{ts} = \sqrt{\frac{8 k_B T_s}{\pi m_s}}, \tag{6}$$

where κ_B is the Boltzmann constant, and m_s is the SiH_4 gas molecule mass.

The gas drag force is taken as;

$$F_n = -\frac{2}{3}\sqrt{2\pi} d_c m_s n_s v_{ts} (v_c - v_s), \tag{7}$$

where v_c is the cluster velocity and v_s is the SiH_4 gas velocity.

The electrostatic force is given by,

$$F_E = qE, \tag{8}$$

where q is the electric charge of cluster, and E is the electric field strength.

As a typical numerical example, the cluster diameter d_c = 5 nm, as shown in Fig. 6, the mass density for Si cluster ρ_c = 2.3 g/cm^3, the translational thermal conductivity κ_t = 19.2 mW/m·K, the temperature gradient in the SiH_4 gas ∇T_s = 250 K/m, the SiH_4 gas molecule mass $m_s = 5.3 \times 10^{-26}$ kg, the SiH_4 gas molecules density $n_s = 1.6 \times 10^{-23}$ m^{-3}, the cluster velocity v_c = 0 m/s, and the SiH_4 gas velocity v_s = 0.18 m/s. Assuming that

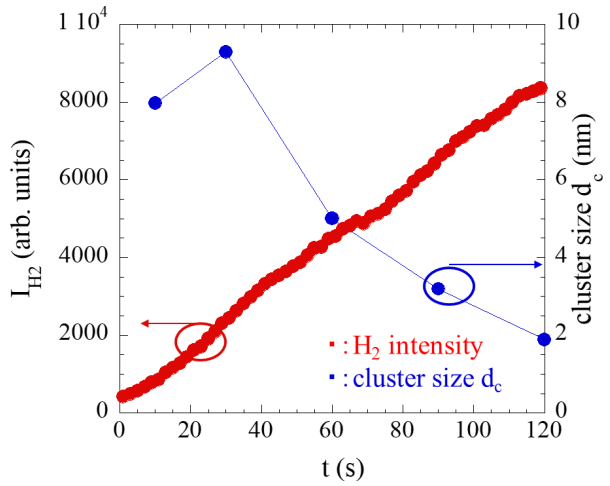

Fig. 7 Time evolution of H_2 intensity and cluster size.

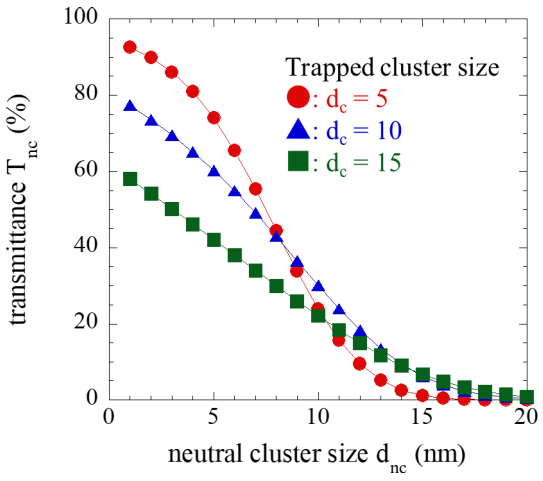

Fig. 8 Theoretical dependence of T_{nc} on d_{nc}.

there is at most one electron attached to the cluster, the electric charge of cluster $q = 1.6 \times 10^{-19}$ C. The self-bias DC voltage V_{dc} is −9.2 V, and the distance between electrodes and QCMs is 20 mm. Thus, assuming the electric field in the downstream region is constant, the electric field $E = 460$ V/m. The forces are,

$$\begin{aligned} F_G &= 1.5 \times 10^{-21}\ \text{N}, \\ F_T &= -1.4 \times 10^{-19}\ \text{N}, \\ F_n &= 2.9 \times 10^{-18}\ \text{N}, \\ F_E &= 7.4 \times 10^{-17}\ \text{N}. \end{aligned} \tag{9}$$

Therefore, gravity, and the thermophoretic force can be disregarded compared with the gas drag force and electrostatic force. Although the electrostatic force is stronger than that of gas flow, they are balanced with each other because the electric field is actually not constant.

Figure 7 shows time evolution of intensity of molecular band of H_2 ($3p^3\Pi_{u-}$—$2s^3\Sigma_{g+}$ around 602 nm [30, 31]) and the cluster size for the gas velocity of 0.18 m/s. In this condition, H_2 is excited by electron collision to H_2 molecules. Thus, this intensity indicates the amount of H_2 in plasmas. The amount of H_2 increases with time. The cluster size is measured by transmission electron microscopy (JEOL JEM-2010). The cluster size decreases with time, because H_2 molecules react with SiH_2 radicals, which contribute to the cluster nucleation, and therefore H_2 molecules inhibit the cluster growth. When the cluster size becomes small, its surface area decreases, and the electron attachment also decreases. This affects the cluster trapping. Actually, as the size of the cluster decreases, R increases as shown in Fig. 3. From these results, in the downstream region of MHDP, we propose the following film deposition process model. During the initial discharge period, clusters are trapped by electrostatic force due to the electron attachment to the clusters, and such trapped clusters lead to low R. Then, small neutral clusters are generated due to the increase of H_2 partial pressure, and some of them are transported to QCMs by the gas flow, and hence R increases.

To discuss the transmittance of neutral clusters passing through a cloud of trapped clusters T_{nc}, we derive the mean free path of neutral cluster in the cluster cloud λ_{nc} as follows;

$$\lambda_{nc} = \frac{1}{n_c \sigma [1 + (m_c/m_{nc})]^{1/2}}, \tag{10}$$

where σ is the total scattering cross section, and m_{nc} is the mass of the neutral cluster. The distribution of free path of neutral cluster $P(l_{nc})$ is expressed as follows;

$$P(l_{nc}) = \frac{1}{\lambda_{nc}} e^{-l_{nc}/\lambda_{nc}}, \tag{11}$$

where l_{nc} is the free path of neutral cluster. Since the transition rate can be regarded as the probability that the free path is greater than or equal to the thickness of the cluster cloud t_{cloud}, the transmittance T_{nc} is,

$$T_{nc} = \int_{t_{cloud}}^{\infty} P(l_{nc}) dl = e^{-t_{cloud}/\lambda_{nc}}. \tag{12}$$

Combining Eqs. (10) and (12), we obtain,

$$T_{nc} = e^{-t_{cloud} n_c \sigma [1+(m_c/m_{nc})]^{1/2}}. \tag{13}$$

Figure 8 shows the theoretical dependence of T_{nc} on neutral cluster size d_{nc} based on Eq. (13), where we employed the thickness of the cluster cloud $t_{cloud} = 10$ mm, the density of cluster cloud $n_c = 2.7 \times 10^{11}$ cm^{-3}, and d_{nc} is the diameter of neutral clusters. When the size of the trapped clusters is the same as the size of the neutral clusters, T_{nc} is 74% at $d_c = 5$ nm, 30% at $d_c = 10$ nm, 6.7% at $d_c = 15$ nm. T_{nc} decreases as the cluster size increases. From this result, trapping large clusters in a high density is suitable for film deposition with low cluster incorporation. The transmittance for around $d_{nc} = 0$ nm can be considered as that of SiH_3 radicals. For $d_c = 15$ nm, T_{nc} of SiH_3 radicals is as

low as 60%, namely, the transport of SiH_3 radicals to the substrate is suppressed. For $d_c = 5$ nm, T_{nc} of $d_{nc} = 10$ nm is 20%, and the T_{nc} of SiH_3 radicals is 90%, which shows an excellent selectivity. Therefore, by separately controlling the sizes of trapped clusters and neutral clusters, this deposition method becomes more effective.

4. Conclusions

We studied the time evolution of *DR* and *R* in the downstream region of MHDPCVD reactor. For the gas velocity = 0.18 m/s, clusters are not driven by gas flow, and are trapped at 7 mm above the substrate, in the initial discharging phase. Trapped clusters suppress the cluster incorporation, and we realized a low *R* of 1.3 with a high *DR* of 0.06 nm/s. Gravity and thermophoretic force are very weak compared with gas drag force and electrostatic force. Thus, electrostatic force balances with gas drag force and cause the cluster trapping phenomenon. We also measured time evolution of H_2 intensity and cluster size. After the cluster trapping, many small clusters are formed due to the increase of H_2. Most of such small clusters are neutral and they are transported to QCMs and eventually, *R* increases.

Acknowledgments

This work was partly supported by JSPS KAKENHI Grant Number JP26246036.

[1] H. Jayakumar, K. Lee, W. Suk Lee, A. Raha, Y. Kim and V. Raghunathan, Proceedings of the 2014 international symposium on Low power electronics and design, ACM (2014).
[2] Y.S. Long, S.T. Hsu and T.C. Wu, PVSC, 2016 IEEE 43rd. IEEE (2016).
[3] K. Tanaka and A. Matsuda, Mater. Sci. Rep. **2**, 139 (1987).
[4] J. Perrin, J. Non-Cryst. Solids **137**, 639 (1991).
[5] J.R. Abelson, Appl. Phys. A: Solids Surf. **56**, 493 (1993).
[6] T. Matsui, A. Bidiville, K. Maejima, H. Sai, T. Koida, T. Suezaki, M. Matsumoto, K. Saito, I. Yoshida and M. Kondo, Appl. Phys. Lett. **106**, 053901 (2015).
[7] T. Matsui, K. Maejima, A. Bidiville, H. Sai, T. Koida, T. Suezaki, M. Matsumoto, K. Saito, I. Yoshida and M. Kondo, Jpn. J. Appl. Phys. **54**, 08KB10 (2015).
[8] H. Sai, T. Matsui and M. Koji, Appl. Phys. Lett. **109**, 183506 (2016).
[9] M. Tsuda, S. Oikawa and K. Sato, J. Chem. Phys. **91**, 6822 (1989).
[10] X.F. Wang, W.Z. Jia, Y.H. Songa, Y.Y. Zhang, Z.L. Dai and Y.N. Wang, Phys. Plasmas **24**, 113503 (2017).
[11] J.P.M. Schmitt, J. Non-Cryst. Solids **59-60**, 649 (1983).
[12] N. Itabashi, N. Nishiwaki, M. Magane, S. Naito, T. Goto, A. Matsuda, C. Yamada and E. Hirota, Jpn. J. Appl. Phys. **29**, L505 (1990).
[13] S. Masaharu, T. Fukuzawa and Y. Watanabe, Jpn. J. Appl. Phys. Part 1 **38**, 4542 (1999).
[14] K. Koga, Y. Matsuoka, K. Tanaka, M. Shiratani and Y. Watanabe, Appl. Phys. Lett. **77**, 2 (2000).
[15] T. Nishimoto, M. Takai, H. Miyahara, M. Kondo and A. Matsuda, J. Non-Cryst. Solids **299-302**, 1116 (2002).
[16] S. Shimizu, H. Miyahara, M. Kondo and A. Matsuda, J. Non-Cryst. Solids **338-340**, 47 (2004).
[17] S. Shimizu, A. Matsuda and M. Kondo, J. Appl. Phys. **101**, 064911 (2007).
[18] M. Shiratani, K. Koga, N. Kaguchi, K. Bando and Y. Watanabe, Thin Solid Films **506-507**, 17 (2006).
[19] K. Koga, M. Kai, M. Shiratani, Y. Watanabe and N. Shikatani, Jpn. J. Appl. Phys. **41**, L168 (2002).
[20] M. Shiratani, K. Koga, S. Iwashita, G. Uchida, N. Itagaki and K. Kamataki, J. Phys. D: Appl. Phys. **44**, 174038 (2011).
[21] S. Toko, Y. Torigoe, K. Keya, H. Seo, N. Itagaki, K. Koga and M. Shiratani, Jpn. J. Appl. Phys. **55**, 01AA19 (2016).
[22] W.M. Nakamura, H. Matsuzaki, H. Sato, Y. Kawashima, K. Koga and M. Shiratani, Surf. Coatings Technol. **205**, S241 (2010).
[23] Y. Kim, K. Hatozaki, Y. Hashimoto, H. Seo, G. Uchida, K. Kamataki, N. Itagaki, K. Koga and M. Shiratani, MRS Proc. **1426**, 307 (2012).
[24] Y. Kim, K. Hatozaki, Y. Hashimoto, G. Uchida, K. Kamataki, N. Itagaki, H. Seo, K. Koga and M. Shiratani, Jpn. J. Appl. Phys. **152**, 01AD01 (2013).
[25] S. Toko, Y. Torigoe, W. Chen, D. Yamashita, H. Seo, N. Itagaki, K. Koga and M. Shiratani, Thin Solid Films **587**, 126 (2015).
[26] K. Keya, T. Kojima, Y. Torigoe, S. Toko, D. Yamashita, H. Seo, N. Itagaki, K. Koga and M. Shiratani, Jpn. J. Appl. Phys. **55**, 07LE03 (2016).
[27] S. Toko, Y. Torigoe, K. Keya, T. Kojima, H. Seo, N. Itagaki, K. Koga and M. Shiratani, Surf. Coat. Technol. **326**, 388 (2017).
[28] S. Nunomura, I. Sakata and M. Kondo, Appl. Phys. Express **6**, 126201 (2013).
[29] S. Nunomura, I. Sakata and M. Kondo, Appl. Phys. Express **10**, 081401 (2017).
[30] K.J. Clay, S.P. Speakman, G.A.J. Amaratunga and S.R.P. Silva, J. Appl. Phys. **79**, 7227 (1996).
[31] M.N. van den Donker, B. Rech, F. Finger, W.M.M. Kessels and van de M.C.M. Sanden, Appl. Phys. Lett. **87**, 263503 (2005).